Effects of solvation and temperature on the energetics of $BiVO_4$ surfaces with varying composition for solar water splitting

Giacomo Melani[1,*#], Wennie Wang[1,2],

Francois Gygi[3], Kyoung-Shin Choi[5], Giulia Galli[1,6,7]

[1]Pritzker School of Molecular Engineering, University of Chicago, IL, USA
[2]McKetta Department of Chemical Engineering, University of Texas at Austin, TX, USA
[3]Department of Computer Science, University of California Davis, CA, USA
[4]Center for Functional Nanomaterials, Brookhaven National Laboratory, NY, USA
[5]Department of Chemistry, University of Wisconsin-Madison, WI, USA
[6]Materials Science Division, Argonne National Laboratory, IL, USA
[7]Department of Chemistry, University of Chicago, IL, USA
#present address: Istituto di Chimica dei Composti Organometallici, Consiglio Nazionale delle Ricerche, Pisa, Italy

ABSTRACT

Photoelectrodes used in solar water splitting must operate in aqueous media. However, many computational studies on oxide photoelectrodes assume vacuum conditions and investigate dry surfaces. To date, computational studies that explicitly compare the dry and solvated photoelectrode energetics at finite temperature and the impact of photoelectrode surface composition, including the presence of surface defects, are lacking. In this study, we used first-principles molecular dynamics simulations to investigate the solvation and thermal effects on the energetics of the $BiVO_4$ (010) surface with different surface compositions and oxygen vacancies, a common defect responsible for the intrinsic n-type behavior of $BiVO_4$. We find that the alignment of the photoelectrode electronic bands with the water redox potentials is modified in the presence of water, similar to other oxides, and that solvation effects and thermal fluctuations are more prominent for Bi-rich surfaces. We also predict that infrared sensitive spectroscopies should be useful to distinguish between the stoichiometric and Bi-rich surfaces. Our results provide a detailed understanding of the behavior of $BiVO_4$ photoanodes operating in aqueous media and are directly comparable with experiments conducted on the stoichiometric and Bi-rich surface.

Oxide semiconductors are interesting materials for use as photoelectrodes in solar water splitting, as they exhibit compositional flexibility and relatively good stability in aqueous environments[1]. Recently, the importance of understanding and optimizing surface structure and composition, in addition to the bulk properties of the oxide photoelectrode, has been demonstrated by various studies[2–9]. For example, we showed that epitaxially-grown $BiVO_4$ (010) photoelectrodes with the stoichiometric (Bi:V ratio of 1:~1) and Bi-rich outermost layer have considerably different surface energetics that directly impact their photoelectrochemical properties; the band edges and work function of the Bi-rich $BiVO_4$ (010) photoelectrode are closer to the vacuum level than those of the stoichiometric surface, resulting in a more pronounced band bending under any applied potential, which in turn leads to a better electron-hole separation and hence to enhanced photocurrent generation[10].

Unlike photoelectrodes used in solid-state solar cells, photoelectrodes used in water-splitting photoelectrochemical cells must operate in aqueous solutions. Thus, an accurate understanding of the impact of the aqueous environment on photoelectrode surfaces requires an understanding of how solvation affects the photoelectrode energetics and electronic properties. However, many computational studies assume vacuum conditions when investigating photoelectrodes. For example, the properties of epitaxially grown $BiVO_4$ (010) photoelectrodes with Bi-rich surfaces were computationally investigated using only dry surfaces[10] while several studies of the solvated stoichiometric ones have appeared in the literature[11–15] .When a ternary oxide with the formula of $A_xB_yO_z$ is prepared, the surface A:B ratio can often be different from the bulk A:B ratio and varies by the synthesis method. Thus, understanding how surfaces with different composition are affected by solvation is of great interest and importance. Another important factor when considering solvation effects is the presence of defects on the photoelectrode surfaces. For example, oxygen vacancies are common defects in n-type oxides such as $BiVO_4$ and their presence on the surface may alter the way the surface and water molecules interact, thereby changing the surface energetics.

In order to address our lack of understanding of solvation effects as a function of surface composition, we investigate the electronic, structural, and vibrational properties of dry and solvated $BiVO_4$ (010) surfaces and we compare results for the stoichiometric and Bi-rich surfaces, with and without oxygen vacancies. The experimentally observed photoelectrochemical properties of $BiVO_4$ (010) with different surface compositions (stoichiometric surface where Bi:V is 1:~1 vs Bi-rich surface) have been well documented[10]. Hence, the computational results reported in this study can be validated by our previous experimental studies, while providing a detailed understanding of the fundamental properties of $BiVO_4$ photoanodes operating in aqueous media.

We carried out first-principles molecular dynamics simulations (FPMD) at the meta-GGA level[16] of theory and investigated the electronic properties of selected snapshots, using hybrid functionals[17]. Specifically, we used the (SCAN) functional and the Qbox code (versions 1.74.2 and 1.75.0)[18] (see SI for details). A total of twelve trajectories of ~ 8 ps each were obtained for the pristine stoichiometric and Bi-rich $BiVO_4$/water interfaces, respectively, for a total simulation time of more than 30 ps in each case. Two additional trajectories of 6 ps

each were generated for each of the $BiVO_4$ interfaces (stoichiometric and Bi-rich) with oxygen vacancies, starting from pre-equilibrated trajectories of the corresponding pristine systems.

We modeled bismuth vanadate in contact with heavy water (64 D_2O molecules) for computational convenience (use of a larger time step than in the case of hydrogenated water) and we used (2 × 2 × 2) symmetric slab models of composition $Bi_{16}V_{16}O_{64}$ and $Bi_{16}V_8O_{56}D_{24}$ (4 BVO layers) and $Bi_{32}V_{32}O_{128}$ and $Bi_{32}V_{24}O_{120}D_{24}$ (8 BVO layers) to represent the stoichiometric and the bismuth-rich surfaces, respectively (see SI for a study of finite size effects). The Bi-rich model used in our previous study[10] was constructed by removing all V atoms from the top-most layer of the stoichiometric surface and terminating the topmost layer with Bi atoms. Experimentally, in order to obtain a Bi-rich sample, the stoichiometric sample is treated in a strongly basic solution for an appropriate duration to remove the top-most vanadium atoms[10]. In such a OH-rich basic aqueous solution, the remaining surface Bi atoms are expected to be hydroxylated. We optimized the geometry of the Bi-rich surface where Bi is terminated with one, two and three OD groups and found that the one with three groups was the most stable. Hence, to closely mimic the experimental Bi-rich sample, the Bi-rich surface model used here consists of stoichiometric $BiVO_4$ layers, covered by four Bi $(OD)_3$ groups on each surface of the slab. The dimensions of the simulation supercell were chosen so that the average water density corresponds to the computed SCAN equilibrium density of 1.05 g/cm^3 (the experimental density for heavy water is 1.11 g/cm^3)[19]. A ball and stick representation of the pristine models used here is shown in Figure 1.

To study the effect of defects on the properties of the $BiVO_4$/water interfaces, we considered the presence of surface oxygen vacancies, building on our previous work where we investigated vacancies in the absence of water[20,21]. We considered the same symmetric slabs described above and removed an oxygen atom from each of the outermost layers, formally removing two oxygen atoms from the slab.

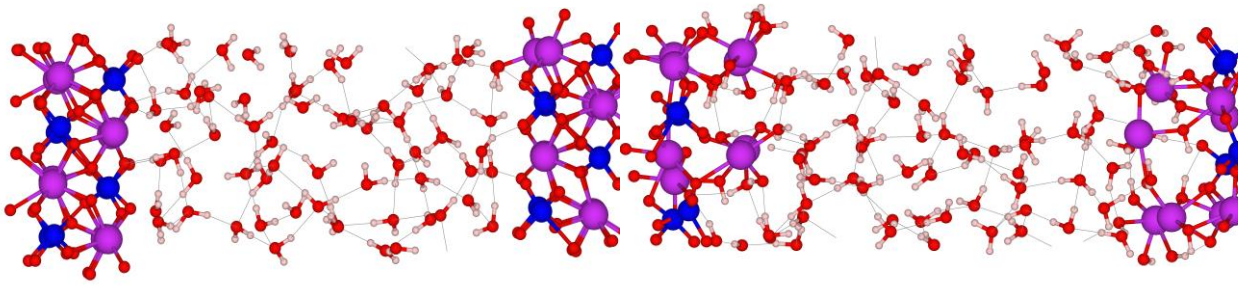

Figure 1 Structural models (balls and stick representation) of the stoichiometric (left) and bismuth-rich $BiVO_4$ (010) surfaces in contact with deuterated water (64 D_2O molecules). We used periodic boundary conditions with a symmetric slab and hence in our supercell two surfaces exposed to water are present. For ease of visualization we show the 64 water molecules at the center of the slab. Color coding: oxygen atoms (red), vanadium (blue), bismuth (purple) and hydrogen (grey).

We discuss the results of our simulations starting from the structural and vibrational properties of water in contact with $BiVO_4$, as obtained from computed vibrational densities of states (VDOS) and infrared (IR) spectra, beginning with the stoichiometric surface.

In agreement with our previous results obtained at the PBE+U[14] level of theory, we found that molecular (i.e., non-dissociative) adsorption of water is energetically preferred with respect to dissociative adsorption on the stoichiometric surface when using the SCAN functional. The SCAN functional yields slightly larger adsorption energies than PBE+U, possibly due to the partial inclusion of short-range van der Waals interactions. We then investigated whether dissociative adsorption is also thermodynamically unfavorable for the fully solvated surface, i.e. when the surface is entirely covered by water molecules. To this end, , we started some of our FPMD simulations from configurations of pre-dissociated D_2O molecules on the surface. We observed that most dissociated fragments present at the interface did recombine to form water molecules, which were then molecularly adsorbed on the surface, in agreement with previous ab-initio simulations[22] and with our own results for one water monolayer[14].

Specifically, on the stoichiometric surface we find that oxygen atoms from water molecules adsorb on the topmost bismuth atoms, interacting with Bi through their lone electronic pairs. Water molecules also adsorb by donating hydrogen bonds to surface oxygen atoms. Interestingly, molecular adsorption does not lead to a full hydration of the surface (i.e., not all surface sites are covered with -OH groups).

In the case of the bismuth-rich (010) surface, where the topmost $Bi(OD)_3$ groups can receive and donate hydrogen bonds to water, the surface-liquid interactions are different from those on the stoichiometric surface. The Bi-rich surface forms temporary hydrogen bonds with water molecules using its terminal deuterated hydroxyl groups which sterically hinder the adsorption of molecular water. While the stoichiometric surface exhibits direct molecular adsorption, the Bi-rich surface features fluctuating hydrogen bonds, which possibly lead to faster diffusion of molecules in the second water layer.

In search of signatures that could be detected experimentally and used to distinguish between the stoichiometric and Bi-rich aqueous interfaces, we computed the vibrational density of states and IR spectra of water at the interface[23]. The VDOS spectrum is obtained from the velocity-velocity autocorrelation function, and it can be easily decomposed into atomic contributions from different species, hence leading to a facile interpretation of the vibrational modes of liquid water in the slab.

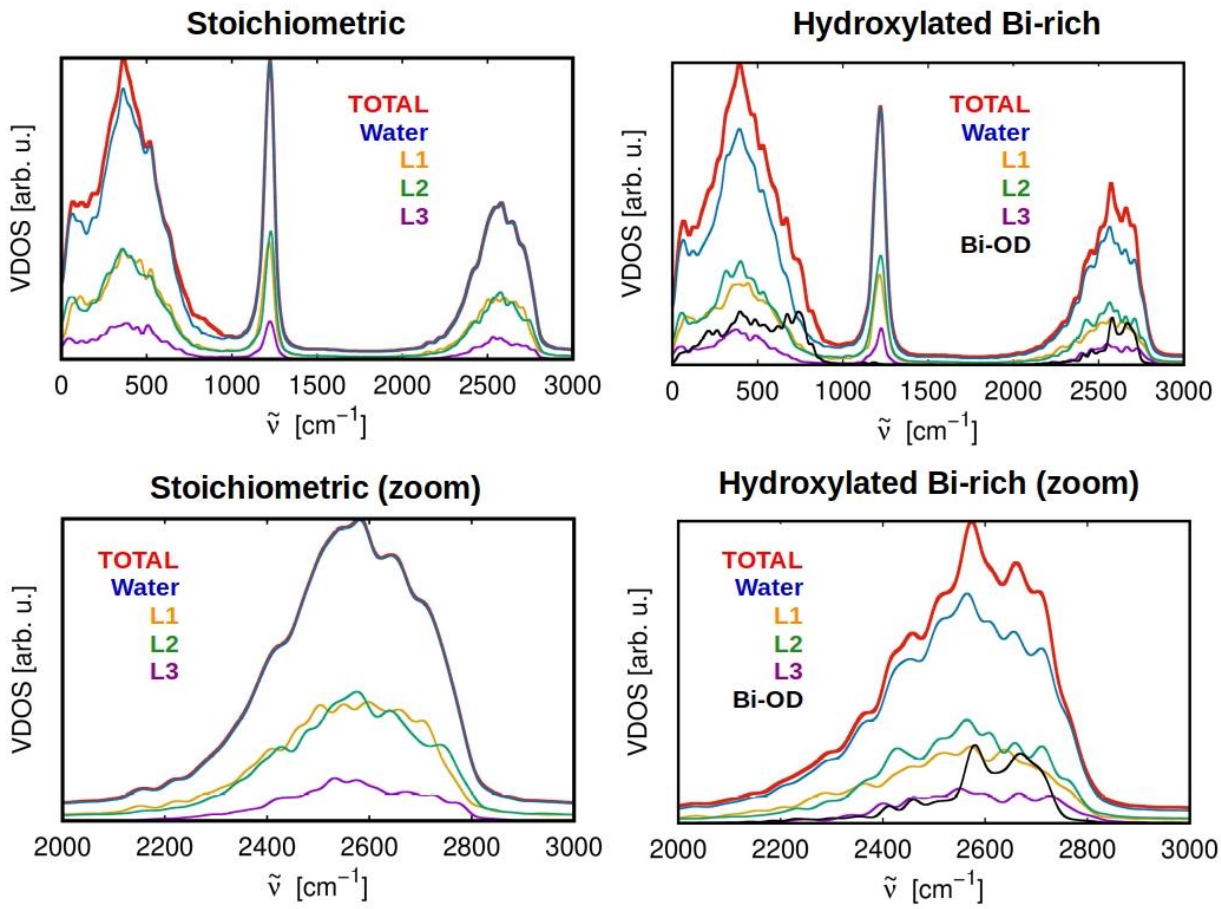

Figure 2 Averaged vibrational densities of states (VDOS) computed from FPMD/SCAN trajectories at 330 K. We show spectra of stoichiometric (left panels) and Bi-rich (right panels) $BiVO_4$ (010) surfaces.. Spectra in the full frequency range and between 2,000-3,000 cm^{-1} are shown in the top and bottom panels, respectively. Raw data are smoothed by applying the Hann window function ($\cos^2(\omega t)$). Color coding: total VDOS (red).In blue, the VDOS for only the D_2O molecules at the interface; in orange, green, and purple, the VDOS for each water layer (L1, L2, L3) in contact with the surface, with L1 being the closest to the $BiVO_4$ surface. In black: VDOS only for $Bi(OD)_3$ groups adsorbed onto the Bi-rich surface.

In Figure 2, we show the VDOS spectra for stoichiometric and bismuth-rich interfaces. In both cases, we observe a band below 1000 cm^{-1} associated with the low-frequency water modes and with lattice vibrations (Bi-O and V-O stretching modes fall within 600 and 900 cm^{-1}); we also observe the well-known D_2O bending peak at about 1250 cm^{-1}. At higher frequencies, in the regime of the O-D stretching modes, we find notable differences between the spectra of the stoichiometric and Bi-rich interfaces. In the stoichiometric surface, the molecular vibrations of adsorbed molecules give rise to a broad band centered below 2600 cm^{-1}, with shoulders at 2700-2800 cm^{-1} associated with asymmetric D_2O stretching and at 2400 cm^{-1} originating from intermolecular hydrogen bonding vibrations. The bismuth-rich interface shows more complex features in the vibrational frequencies corresponding to the O-D stretching modes, originating from the occurrence of both water and $Bi(OD)_3$ vibrations: O-D stretching modes from surface bismuth hydroxide groups contribute to the peaks at high

frequency close to 2700 cm^{-1}, with lesser impact to the hydrogen bond modes below 2500 cm^{-1}. Although less prominent than in the stretching band, the bismuth hydroxide vibrations also differ in the lower-frequency part of the VDOS spectrum, yielding an additional shoulder to the 800-900 cm^{-1} band, which is consistent with Bi-O stretching modes.

As a further step to investigate the vibrational properties of solvated $BiVO_4$ surfaces, we report infrared spectra obtained from FPMD, where vibrational intensities were calculated by computing the dipole-dipole autocorrelation function obtained from Maximally-Localized Wannier Functions (MLWFs)[19]; the IR spectrum at finite temperature was obtained as:

$$A(\omega)\, n(\omega) = \frac{2\pi\omega^2\beta}{3cV}\int_{-\infty}^{+\infty}\langle \underline{M}(0)\cdot\underline{M}(t)\rangle\, e^{-i\omega t}dt \qquad (1)$$

where $\underline{M}$ is the total dipole moment obtained from MLWFs, β, V c, A(ω), n(ω) are the Boltzmann inverse temperature, the speed of light, the absorption coefficient and the refractive index, respectively.

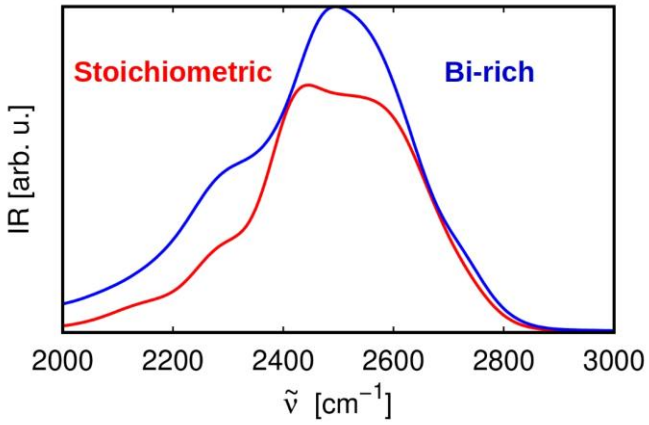

Figure 3 Infrared (IR) spectrum computed from FPMD/SCAN trajectories (six each for the stoichiometric and hydroxylated Bi-rich surfaces) at 330 K for solvated $BiVO_4$ (010). Color coding: stoichiometric interface (red), bismuth-rich (blue). Raw data are smoothed with a Gaussian windowing of 40 cm^{-1}.

Similar to the VDOS spectra, the computed IR response in the O-D stretching region show differences between the stoichiometric and bismuth-rich interfaces, originating from the presence of $Bi(OD)_3$ groups. Compared to the VDOS, the IR intensities are slightly different, but again exhibit a main band centered around 2500-2600 cm^{-1} and shoulders at 2800 cm^{-1} and 2400 cm^{-1}, respectively. Our calculations show that differences between Bi-rich and stoichiometric $BiVO_4$ should be detectable in surface-sensitive IR measurements, such as sum frequency generation (SFG) measurements[24]. If these experiments are feasible, they are expected to be a useful tool to assess the type of aqueous interfaces formed under different experimental conditions.

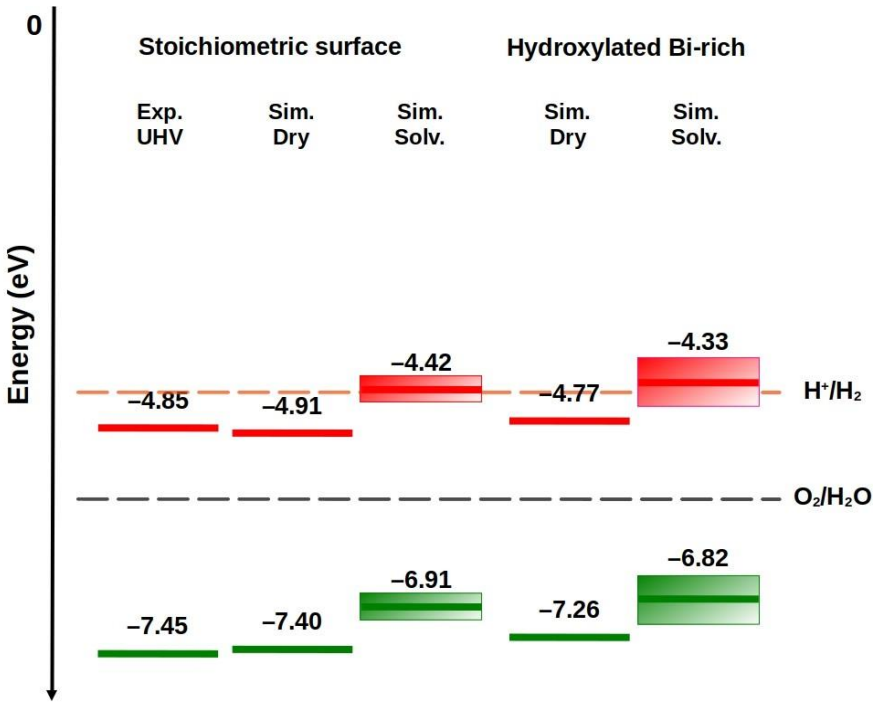

Figure 4 Band alignment of the valence band maxima (VBM, in green) and conduction band minima (CBM, in red) with respect to vacuum level for stoichiometric and hydroxylated- Bi-rich $BiVO_4$ (010). We report experimental values of single-crystalline $BiVO_4$ obtained in ultra-high-vacuum conditions (Exp. UHV) from Refs.[10,32]. and results obtained from first-principles simulations (Sim.) for the dry and solvated (Solv.) stoichiometric and Bi-rich surfaces. Electronic energy levels are computed at the DDH level of theory on 20 snapshots obtained from SCAN/FPMD trajectories at 330 K for both systems. Thermal fluctuations of V(C)BM values are indicated with green and red rectangles, yielding a 150 and 280 meV spread for the stoichiometric and bismuth-rich interfaces, respectively.

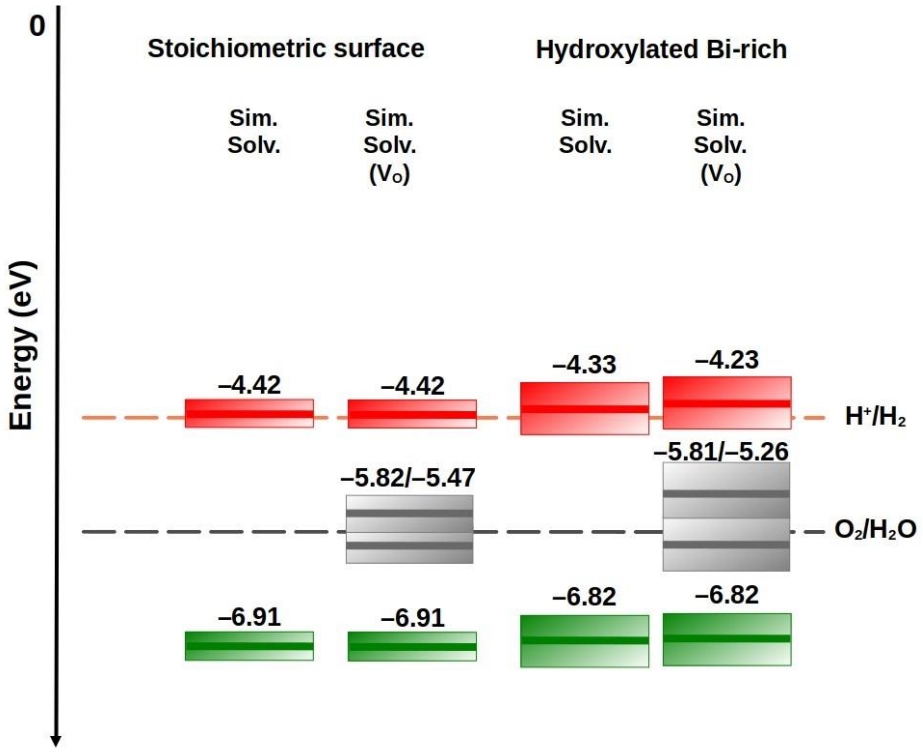

Figure 5 Band alignment of the valence band maxima (VBM, in green) and conduction band minima (CBM, in red) relative to the vacuum level for solvated (Solv.) stoichiometric and hydroxylated- Bi-rich $BiVO_4$ (010), in the presence of oxygen vacancies (V_O), as obtained from first-principles simulations (Sim.). Electronic energy levels are computed at the DDH level of theory from 20 snapshots obtained from SCAN/FPMD trajectories at 330 K for both systems. Thermal fluctuations of V(C)BM values and defect levels are indicated with green, red and gray rectangles, respectively. The defect levels were computed at the SCAN level of theory, and they were positioned relative to the top of the vacuum-referenced valence band obtained in Fig.4.

We now turn to the discussion of the electronic properties of solvated stoichiometric and Bi-rich surfaces, in particular the effect played by solvation and surface composition on the band edge positions of the photoelectrode.

Following previous work[10,12,14,21,25–30], we determined the absolute valence band maximum (VBM) and conduction band minimum (CBM) positions with respect to the vacuum level, and we then aligned them to the water electrochemical potentials (see SI for details).

Figures 4 and 5 summarize our results for pristine and defective $BiVO_4$, respectively; the electronic structure was obtained using the DDH hybrid functional on SCAN trajectories and using 8 layer slabs to represent the surface (see SI). Note that we adopted corrections due to spin-orbit coupling, excitonic and nuclear quantum effects, which for $BiVO_4$ have been shown to lead to a shift (Δ) in the band edge positions (ΔVBM = +0.50 eV, ΔCBM = –0.43 eV). Such corrections are numerically different from those previously reported[21,31] as thermal fluctuations are already included in our finite-temperature FPMD simulations and were thus omitted from the corrections proposed in Ref. 21.

We start by describing the surfaces in the absence of defects. Figure 4 compares the band alignments of stoichiometric and hydroxylated Bi-rich $BiVO_4$ (010) with dry and solvated surfaces (see SI) so that the effects of solvation on the band edge positions are explicitly shown.

For dry, UHV-like conditions, we find that the VBM of the stoichiometric surface is located at 7.40 eV from vacuum, in agreement with previously reported values[21] computed at the PBE+U(2.7 eV) level and also with photo-emission experiments (7.45 eV)[32]. When considering a solvated stoichiometric surface, we find that the VBM moves up to 6.91 eV and the CBM moves up to 4.42 eV. Such a shift in the electronic band edges due to solvation is consistent with what has been reported for other oxides[33].

We note that in our previous study[10], the positions of the VBM and CBM levels of the dry bismuth-rich surface were calculated without hydroxylation or solvation, and hence their positions were unrealistically close to the vacuum level (at 4.63 eV and 2.49 eV from vacuum, respectively); in particular, the VBM position was even higher (less positive in the reversible hydrogen electrode scale) than that of the water oxidation potential, which is unrealistic. However, when the surface is hydroxylated, namely terminated by $Bi(OD)_3$, we find that the VBM and CBM levels are lowered and are positioned closer to but not above the oxygen evolution reaction (OER) potential. At the same time, the CBM and VBM of the dry, hydroxylated Bi-rich surface are still slightly higher than those of the dry stoichiometric surface (Figure 4). For example, the VBM of the dry, hydroxylated Bi-rich surface is higher by 0.14 eV: this value is comparable to the experimentally observed difference (0.15 eV) between the VBM levels of these two samples, which was determined by XPS under vacuum conditions[10].

When the surface is fully solvated, the VBM and CBM levels of the hydroxylated Bi-rich surface moves up slightly closer to the vacuum level as in the case of the stoichiometric sample, and hence they remain higher than those of the solvated stoichiometric surface, consistent with the experimental results discussed in detail below.

The CBM of the solvated, hydroxylated Bi-rich surface shown in Figure 4 is slightly above the HER potential (–4.44 eV)[34]. We note that this result was obtained by carrying out MD simulations of a Bi-rich surface with the top-most layer having only Bi and no V (i.e., equivalent to having 4 Bi atoms at the top-most layer). However, in experiments, Bi-rich samples can still contain some V atoms on the surface and the coordination of Bi may be different from that used in our calculations. We expect that both the surface Bi:V ratio and their detailed coordination environments can impact the exact CBM position of experimental samples. For example, the experimental Bi-rich sample prepared in our previous study[10] had the Bi:V ratio of 79:21, and our previous calculations showed that the band edge positions shift closer to the vacuum and vary linearly with increasing Bi:V ratio[10]. Therefore, we repeated some of our calculations using 75% Bi-rich substrates and we observed a slight lowering of the CBM below the hydrogen evolution potential, consistent with the expectations that Bi-rich surfaces may indeed contain some V atoms at the surface and that

the $BiVO_4$ surface is not HER active. We also observed a modest lowering of the VBM when decreasing the Bi-concentration at the surface.

It is important to note that thermal fluctuations have a larger influence on the electronic structure of the Bi-rich surface relative to the stoichiometric one, as shown in Figure 4. This difference is shown by the width of the colored rectangles, whose edges show the energetic range of the fluctuations. The increased amplitude in the Bi-rich surface is due to the presence of Bi-OH groups and dynamically gives rise to a more favorable positions of the CBM and VBM for water splitting.

Next, we consider the effect of the surface O vacancy (V_O) on the solvation effects. In $BiVO_4$, oxygen vacancies are considered a common source of n-type dopants, as in many semiconducting oxides. In a previous work by our group[21], an extensive analysis of oxygen vacancies in bulk and surface bismuth vanadate was reported, shedding light on the role of this type of defect on the electronic structure of $BiVO_4$.

Here, we considered a neutral Vo where an oxygen atom is removed from a VO_4^{3-} anion and the remaining VO_3^{3-} species has two unpaired electrons in the vanadium 3*d*-orbitals (V^{3+} with a d^2 electronic configuration), making the oxygen vacancy an n-type dopant. Due to this change in composition and electronic structure, the atoms surrounding the anion vacancy undergoes a structural deformation at finite temperature, and the geometry is stabilized by hydrogen bonding with D_2O molecules.

Figure 5 compares the band alignments of the solvated surfaces of stoichiometric and hydroxylated Bi-rich $BiVO_4$ (010) without and with V_O so that the effects of V_O on the band edge positions are explicitly shown. First, the presence of V_O does not shift the VBM and CBM of the stoichiometric surface. However, the presence of V_O on the Bi-rich surface further shifts the CBM toward the vacuum level by 0.1 eV while the VBM remains the same. This shows that the effect of Vo on the solvation effects vary with the surface composition. This also means that in order to most accurately elucidate the effect of V_O on the solvation effects for any given oxide photoelectrode[35], knowing the surface composition and using a surface model mimicking the experimental surface is critical to obtain the most meaningful results.

The band diagrams of the solvated models with V_O (Figure 5) are those most relevant to use to interpret the experimentally observed photoelectrochemical behavior of the two samples under illumination. In our previous study, we compared $BiVO_4$ (010) photoelectrodes with stoichiometric and Bi-rich surfaces for photoelectrochemical sulfite oxidation[10]. Sulfite is a hole scavenger with fast interfacial oxidation kinetics unlike water whose oxidation kinetics on the $BiVO_4$ surface are much slower[32,36]. Therefore, during photoelectrochemical sulfite oxidation the surface recombination of holes can be assumed to be negligible. As a result, the photocurrent onset potential for sulfite oxidation can be considered as the apparent flat band potential of the photoanode[36]. Furthermore, the difference in photocurrent between the two samples can be directly related to the difference in the number of surface-reaching holes, which results from the effect of surface composition on interfacial energetics and band bending. Our previous experimental results showed that the sample with the Bi-rich surface

has a more negative photocurrent onset potential and significantly enhances photocurrent for sulfite oxidation[10]. Previously, these differences were interpreted with the band diagrams obtained without including the effect of hydroxylation of the Bi-rich surface, the presence of Vo, or solvation effects. Qualitatively, our previous and current results both show that the Bi-rich surface has band edge positions and work function closer to the vacuum level than those of the stoichiometric surface. This qualitatively explains the fact that the sample with the Bi-rich surface is expected to have a greater degree of band bending under any given potential, thereby leading to a greater degree of electron-hole pair separation, compared to the stoichiometric surface, and thus generating an enhanced photocurrent for sulfite oxidation. However, previous calculations were not quantitatively accurate and neglected solvation and defect effects. The current results reported in Figure 5 show more accurate band positions for the two samples with a difference that explains the experimentally observed behaviors.

As seen in Figure 5, two in-gap states corresponding to the two oxygen vacancies introduced appear for both systems, with the spacing between these defect levels depending on the surface composition. For the stoichiometric interface, the defect levels are separated by about 350 meV, while in the Bi-rich case they are separated by 800 meV and are subject to larger thermal fluctuations. Both defect levels are occupied in the case of neutral vacancies, formally shifting the Fermi level upward.

We note that when $BiVO_4$ is used as a photoanode for water oxidation in an aqueous solution under illumination, some of the defect levels will be emptied, due to the recombination of the electrons in these levels with the photogenerated holes in the VBM. If the resulting empty defect levels are located below the OER potential, they may mediate the electron transfer from water to the VB of $BiVO_4$ (equivalent to hole transfer from the VB of $BiVO_4$ to water) during photooxidation of water, affecting the rate of OER. Physically, the V_O may also offer a site where water adsorbs differently than on the non-defective surface (i.e., by dissociative adsorption), affecting the OER mechanism and potentially allowing for a more facile water oxidation[12–14].

In reality, however, the $BiVO_4$ surface is poorly catalytic for OER and is always paired with an oxygen evolution catalyst when used for solar water oxidation[37]. Then, the position of the defect levels relative to the redox level of the catalytic center in the OER catalyst will be important as the position of the defect levels can impact how well the holes can be transferred from $BiVO_4$ to the OER catalyst, and what fraction of the holes will be lost at the interface due to interfacial electron-hole recombination. The impact of the defect levels studied here (Figure 5) and their interaction with OER catalysts merits further investigation, and it is expected to vary depending on the choice of the OER catalyst. Nevertheless, our study clearly demonstrates that even with the same type of defect (in this case, V_O), the solvation effects on the positions and fluctuations of the defect levels and band edges vary depending on the surface composition of $BiVO_4$, all of which will influence differently the OER performance and the way $BiVO_4$ photoanodes interact with an OER catalyst.

In summary, we have investigated how solvation, and the presence of defects influence the structural, vibrational, and electronic structure of the $BiVO_4$ (010) surface, as a function of the surface composition. While most computational studies of $BiVO_4$ surfaces have been limited to static calculations and solvation properties have been studied in only a few papers for stoichiometric surfaces, here we investigated also Bi-rich surfaces, known experimentally to yield photoelectrodes of superior performance. Our results, obtained with first-principles MD simulations, reveal the beneficial effect of solvation in leading to a more favorable position of the VBM and CBM with respect to the OER potential in comparison to those of the dry surfaces. The presence of V_O in combination with thermal fluctuations also contribute to a more favorable electronic structure of Bi-rich $BiVO_4$ (010) for solar water splitting. Our results also provide accurate band positions that can explain the previously observed experimental result where $BiVO_4$ (010) with the Bi-rich surface exhibited a pronounced band bending and enhanced electron-hole separation, resulting in higher photocurrent generation compared to $BiVO_4$ (010) with the stoichiometric surface. Finally, we presented calculated IR spectra indicating that the differences between the stoichiometric and Bi-rich surfaces should be detectable in IR-sensitive spectroscopies, such as sum-frequency generation techniques. The realistic models of solvated and defective surfaces obtained in this work will serve as a basis of further studies of $BiVO_4$ photoelectrodes interfaced with protective layers and with catalysts, and as a template for understanding the aqueous interface of other complex oxide surfaces.

Acknowledgements

We thank Chenyu Zhou and Mingzhao Liu for many useful discussions and Jorge Sofo and Alessandro Fortunelli for discussions and continuous support. This work was funded by the National Science Foundation (NSF) under grant no. CHE-2054986.

References

(1) Lee, D. K.; Lee, D.; Lumley, M. A.; Choi, K.-S. Progress on Ternary Oxide-Based Photoanodes for Use in Photoelectrochemical Cells for Solar Water Splitting. *Chem. Soc. Rev.* **2019**, *48* (7), 2126–2157. https://doi.org/10.1039/C8CS00761F.

(2) Sharp, I. D.; Cooper, J. K.; Toma, F. M.; Buonsanti, R. Bismuth Vanadate as a Platform for Accelerating Discovery and Development of Complex Transition-Metal Oxide Photoanodes. *ACS Energy Lett.* **2017**, *2* (1), 139–150. https://doi.org/10.1021/acsenergylett.6b00586.

(3) Zachäus, C.; Abdi, F. F.; Peter, L. M.; Van De Krol, R. Photocurrent of $BiVO_4$ Is Limited by Surface Recombination, Not Surface Catalysis. *Chem. Sci.* **2017**, *8* (5), 3712–3719. https://doi.org/10.1039/C7SC00363C.

(4) Nguyen, T. D.; Nguyen, V.-H.; Nanda, S.; Vo, D.-V. N.; Nguyen, V. H.; Van Tran, T.; Nong, L. X.; Nguyen, T. T.; Bach, L.-G.; Abdullah, B.; Hong, S.-S.; Van Nguyen, T. BiVO4 Photocatalysis Design and Applications to Oxygen Production and Degradation of Organic Compounds: A Review. *Environ. Chem. Lett.* **2020**, *18* (6), 1779–1801. https://doi.org/10.1007/s10311-020-01039-0.

(5) Zhou, L.; Shinde, A.; Guevarra, D.; Haber, J. A.; Persson, K. A.; Neaton, J. B.; Gregoire, J. M. Successes and Opportunities for Discovery of Metal Oxide Photoanodes for Solar Fuels Generators. *ACS Energy Lett.* **2020**, *5* (5), 1413–1421. https://doi.org/10.1021/acsenergylett.0c00067.
(6) Kim, T. W.; Ping, Y.; Galli, G. A.; Choi, K. S. Simultaneous Enhancements in Photon Absorption and Charge Transport of Bismuth Vanadate Photoanodes for Solar Water Splitting. *Nat. Commun.* **2015**, *6*. https://doi.org/10.1038/ncomms9769.
(7) Ding, K.; Chen, B.; Fang, Z.; Zhang, Y.; Chen, Z. Why the Photocatalytic Activity of Mo-Doped BiVO4 Is Enhanced: A Comprehensive Density Functional Study. *Phys. Chem. Chem. Phys.* **2014**, *16* (26), 13465. https://doi.org/10.1039/c4cp01350f.
(8) Tachikawa, T.; Ochi, T.; Kobori, Y. Crystal-Face-Dependent Charge Dynamics on a $BiVO_4$ Photocatalyst Revealed by Single-Particle Spectroelectrochemistry. *ACS Catal.* **2016**, *6* (4), 2250–2256. https://doi.org/10.1021/acscatal.6b00234.
(9) Zhu, J.; Fan, F.; Chen, R.; An, H.; Feng, Z.; Li, C. Direct Imaging of Highly Anisotropic Photogenerated Charge Separations on Different Facets of a Single $BiVO_4$ Photocatalyst. *Angew. Chem. Int. Ed.* **2015**, *54* (31), 9111–9114. https://doi.org/10.1002/anie.201504135.
(10) Lee, D.; Wang, W.; Zhou, C.; Tong, X.; Liu, M.; Galli, G.; Choi, K. S. The Impact of Surface Composition on the Interfacial Energetics and Photoelectrochemical Properties of BiVO4. *Nat. Energy* **2021**, *6* (3), 287–294. https://doi.org/10.1038/s41560-021-00777-x.
(11) Ambrosio, F.; Wiktor, J.; Pasquarello, A. PH-Dependent Surface Chemistry from First Principles: Application to the BiVO4(010)-Water Interface. *ACS Appl. Mater. Interfaces* **2018**, *10* (12), 10011–10021. https://doi.org/10.1021/acsami.7b16545.
(12) Wiktor, J.; Pasquarello, A. Electron and Hole Polarons at the BiVO4-Water Interface. *ACS Appl. Mater. Interfaces* **2019**, *11* (20), 18423–18426. https://doi.org/10.1021/acsami.9b03566.
(13) Hermans, Y.; Murcia-López, S.; Klein, A.; Jaegermann, W. BiVO4 Surface Reduction upon Water Exposure. *ACS Energy Lett.* **2019**, *4* (10), 2522–2528. https://doi.org/10.1021/acsenergylett.9b01667.
(14) Wang, W.; Favaro, M.; Chen, E.; Trotochaud, L.; Bluhm, H.; Choi, K. S.; Van De Krol, R.; Starr, D. E.; Galli, G. Influence of Excess Charge on Water Adsorption on the BiVO4(010) Surface. *J. Am. Chem. Soc.* **2022**, *144* (37), 17173–17185. https://doi.org/10.1021/jacs.2c07501.
(15) Tao, J.; Liu, G.; Liu, T. Ab Initio Molecular Dynamics Simulation the Electron and Hole Polarons at the Interface between Water and the Surfaces of $BiVO_4$. *J. Phys. Chem. C* **2024**, *128* (13), 5680–5685. https://doi.org/10.1021/acs.jpcc.3c06847.
(16) Sun, J.; Ruzsinszky, A.; Perdew, J. P. Strongly Constrained and Appropriately Normed Semilocal Density Functional. *Phys. Rev. Lett.* **2015**, *115* (3), 036402. https://doi.org/10.1103/PhysRevLett.115.036402.
(17) Skone, J. H.; Govoni, M.; Galli, G. Self-Consistent Hybrid Functional for Condensed Systems. *Phys. Rev. B* **2014**, *89* (19), 195112. https://doi.org/10.1103/PhysRevB.89.195112.
(18) Gygi, F. Architecture of Qbox: A Scalable First-Principles Molecular Dynamics Code. *IBM J. Res. Dev.* **2008**, *52* (1.2), 137–144. https://doi.org/10.1147/rd.521.0137.
(19) Lacount, M. D.; Gygi, F. Ensemble First-Principles Molecular Dynamics Simulations of Water Using the SCAN Meta-GGA Density Functional. *J. Chem. Phys.* **2019**, *151* (16). https://doi.org/10.1063/1.5124957.
(20) Seo, H.; Ping, Y.; Galli, G. Role of Point Defects in Enhancing the Conductivity of BiVO4. *Chem. Mater.* **2018**, *30* (21), 7793–7802. https://doi.org/10.1021/acs.chemmater.8b03201.
(21) Wang, W.; Strohbeen, P. J.; Lee, D.; Zhou, C.; Kawasaki, J. K.; Choi, K. S.; Liu, M.; Galli, G. The Role of Surface Oxygen Vacancies in BiVO4. *Chem. Mater.* **2020**, *32* (7), 2899–2909. https://doi.org/10.1021/acs.chemmater.9b05047.
(22) Oshikiri, M.; Boero, M. Water Molecule Adsorption Properties on the BiVU4 (100) Surface. *J. Phys. Chem. B* **2006**, *110* (18), 9188–9194. https://doi.org/10.1021/jp0555100.

(23) Huang, P.; Pham, T. A.; Galli, G.; Schwegler, E. Alumina(0001)/Water Interface: Structural Properties and Infrared Spectra from First-Principles Molecular Dynamics Simulations. *J. Phys. Chem. C* **2014**, *118* (17), 8944–8951. https://doi.org/10.1021/jp4123002.
(24) Calegari Andrade, M. F.; Ko, H.-Y.; Car, R.; Selloni, A. Structure, Polarization, and Sum Frequency Generation Spectrum of Interfacial Water on Anatase TiO_2. *J. Phys. Chem. Lett.* **2018**, *9* (23), 6716–6721. https://doi.org/10.1021/acs.jpclett.8b03103.
(25) Ambrosio, F.; Miceli, G.; Pasquarello, A. Redox Levels in Aqueous Solution: Effect of van Der Waals Interactions and Hybrid Functionals. *J. Chem. Phys.* **2015**, *143* (24). https://doi.org/10.1063/1.4938189.
(26) Guo, Z.; Ambrosio, F.; Chen, W.; Gono, P.; Pasquarello, A. Alignment of Redox Levels at Semiconductor-Water Interfaces. *Chem. Mater.* **2018**, *30* (1), 94–111. https://doi.org/10.1021/acs.chemmater.7b02619.
(27) Hörmann, N. G.; Guo, Z.; Ambrosio, F.; Andreussi, O.; Pasquarello, A.; Marzari, N. Absolute Band Alignment at Semiconductor-Water Interfaces Using Explicit and Implicit Descriptions for Liquid Water. *Npj Comput. Mater.* **2019**, *5* (1). https://doi.org/10.1038/s41524-019-0238-4.
(28) Anh Pham, T.; Li, T.; Nguyen, H. V.; Shankar, S.; Gygi, F.; Galli, G. Band Offsets and Dielectric Properties of the Amorphous Si 3N4/Si(100) Interface: A First-Principles Study. *Appl. Phys. Lett.* **2013**, *102* (24). https://doi.org/10.1063/1.4811481.
(29) Pham, T. A.; Lee, D.; Schwegler, E.; Galli, G. Interfacial Effects on the Band Edges of Functionalized Si Surfaces in Liquid Water. *J. Am. Chem. Soc.* **2014**, *136* (49), 17071–17077. https://doi.org/10.1021/ja5079865.
(30) Gaiduk, A. P.; Govoni, M.; Seidel, R.; Skone, J. H.; Winter, B.; Galli, G. Photoelectron Spectra of Aqueous Solutions from First Principles. *J. Am. Chem. Soc.* **2016**, *138* (22), 6912–6915. https://doi.org/10.1021/jacs.6b00225.
(31) Wiktor, J.; Reshetnyak, I.; Ambrosio, F.; Pasquarello, A. Comprehensive Modeling of the Band Gap and Absorption Spectrum of BiVO4. *Phys. Rev. Mater.* **2017**, *1* (2). https://doi.org/10.1103/PhysRevMaterials.1.022401.
(32) Cooper, J. K.; Gul, S.; Toma, F. M.; Chen, L.; Glans, P. A.; Guo, J.; Ager, J. W.; Yano, J.; Sharp, I. D. Electronic Structure of Monoclinic BiVO4. *Chem. Mater.* **2014**, *26* (18), 5365–5373. https://doi.org/10.1021/cm5025074.
(33) Ping, Y.; Sundararaman, R.; Goddard, W. A. Solvation Effects on the Band Edge Positions of Photocatalysts from First Principles. *Phys. Chem. Chem. Phys.* **2015**, *17* (45), 30499–30509. https://doi.org/10.1039/c5cp05740j.
(34) Trasatti, S. The Absolute Electrode Potential: An Explanatory Note (Recommendations 1986). *Pure Appl. Chem.* **1986**, *58* (7), 955–966. https://doi.org/10.1351/pac198658070955.
(35) Gerosa, M.; Gygi, F.; Govoni, M.; Galli, G. The Role of Defects and Excess Surface Charges at Finite Temperature for Optimizing Oxide Photoabsorbers. *Nat. Mater.* **2018**, *17* (12), 1122–1127. https://doi.org/10.1038/s41563-018-0192-4.
(36) Govindaraju, G. V.; Wheeler, G. P.; Lee, D.; Choi, K. S. Methods for Electrochemical Synthesis and Photoelectrochemical Characterization for Photoelectrodes. *Chem. Mater.* **2017**, *29* (1), 355–370. https://doi.org/10.1021/acs.chemmater.6b03469.
(37) Hilbrands, A. M.; Zhang, S.; Zhou, C.; Melani, G.; Wi, D. H.; Lee, D.; Xi, Z.; Head, A. R.; Liu, M.; Galli, G.; Choi, K.-S. Impact of Varying the Photoanode/Catalyst Interfacial Composition on Solar Water Oxidation: The Case of $BiVO_4$ (010)/FeOOH Photoanodes. *J. Am. Chem. Soc.* **2023**, *145* (43), 23639–23650. https://doi.org/10.1021/jacs.3c07722.